




# Experimental study of a microsecond-pulsed cold plasma jet

S. Mashayekh<sup>1,a</sup>, N. Cvetanović<sup>2,b</sup> , G. B. Sretenović<sup>3,c</sup>, B. M. Obradović<sup>3,d</sup>, Z. Liu<sup>1,e</sup>, K. Yan<sup>1,f</sup>, and M. M. Kuraica<sup>3,g</sup>

<sup>1</sup> Institute of Industrial Ecology and Environment, Zhejiang University, Hangzhou 310007, China

<sup>2</sup> University of Belgrade, Faculty of Transport and Traffic Engineering, 11000 Belgrade, Serbia

<sup>3</sup> University of Belgrade, Faculty of Physics, 11001 Belgrade, Serbia

Received 7 March 2023 / Accepted 30 May 2023 / Published online 22 June 2023  
© The Author(s), under exclusive licence to EDP Sciences, SIF and Springer-Verlag GmbH Germany, part of Springer Nature 2023

**Abstract.** Cold plasma jets at atmospheric pressure have become the standard reactors used for treatment of various biosamples and other application. The object of this experimental study is one such reactor powered by a short-pulse voltage with a rise time  $\approx 400$  ns, operating with helium gas. The main aim of the investigation was to obtain the data on the jet streamer space–time development and plasma parameters near the target. Axial and radial structure was examined along with gas temperature and electric field above the target. Results show a comparably fast streamer progression ( $10^5$  m/s) with strong electric field in the period of maximum current (33 kV/cm). These characteristic features can be attributed to the fast rise of the voltage pulse.

## 1 Introduction

In the last decade, nonthermal, atmospheric pressure discharges have been adopted as the future of plasma application due to their many advantages, see for instance [1, 2]. A subtype of these plasma reactors are low-temperature plasma jets, commonly known as atmospheric pressure plasma jets (APPJs), usually obtained in the flow of inert gases [3–5]. In a number of publications, helium plasma jets are especially investigated as candidates for treatment of biomedical and other samples, see for instance [4–7]. The efficiency of APPJs in interaction with various types of samples has so far been confirmed in: wound healing, pollutants removal, antimicrobial effects, treatment of cancer cells, etc. [6, 8, 9]. These effects on biosamples are mostly realized via intensive production of reactive oxygen and

nitrogen species (RONS), [4, 9, 10]. Transient electric field, generated in the plasma, was also found to be important for treatment of biomedical samples [11–14].

The APPJs have also been extensively studied from the standpoint of plasma investigation, both through modeling and experiment, see for instance [3, 15–21]. Knowledge of plasma parameters and understanding of involved processes is important for successful optimization and control of its action on the samples. The jet discharge is commonly based on a flow of an inert gas passing through a dielectric tube, where a barrier discharge is formed. Then, a plasma plume emerges from the tube nozzle into ambient air, with or without a grounded target. Due to its rapid progression, this type of plasma was perceived as a “plasma bullet.” Presently, it is well explained and successfully modeled as a guided streamer propagating rapidly via a strong ionizing front at the head of the streamer—a narrow, strong electric field region [17, 21, 22]. Specifically, it was concluded that the ionization front maintains the connection with the DBD ignition zone via a recombining plasma column [23–25].

Interesting feature of the atmospheric plasma jets is the mixing of the propagating feeding gas with the surrounding air, within the plasma plume. This effectively changes the gas composition with distance. Additionally, it was found that that electro-hydrodynamic and thermal mechanisms play a role in the rare gas flow and its mixing with environment, see [26] and references therein.

Guest editors: Bratislav Obradović, Jovan Cvetić, Dragana Ilić, Vladimir Srećković, Sylwia Ptasinska.

T.I.: Physics of Ionized Gases and Spectroscopy of Isolated Complex Systems: Fundamentals and Applications.

<sup>a</sup> e-mail: [amir4522@zju.edu.cn](mailto:amir4522@zju.edu.cn)

<sup>b</sup> e-mail: [nikola@ff.bg.ac.rs](mailto:nikola@ff.bg.ac.rs) (corresponding author)

<sup>c</sup> e-mail: [sretenovic@ff.bg.ac.rs](mailto:sretenovic@ff.bg.ac.rs)

<sup>d</sup> e-mail: [obrat@ff.bg.ac.rs](mailto:obrat@ff.bg.ac.rs)

<sup>e</sup> e-mail: [zliu@zju.edu.cn](mailto:zliu@zju.edu.cn)

<sup>f</sup> e-mail: [kyan@zju.edu.cn](mailto:kyan@zju.edu.cn)

<sup>g</sup> e-mail: [kuki@ff.bg.ac.rs](mailto:kuki@ff.bg.ac.rs)

Plasma parameters were shown to depend on: plume length, working gas, gas flow rate, target material, shape of voltage waveform, etc. It was found that pulse voltage rise time strongly influences the streamer velocity and electric characteristics of the jet [22].

One of such sources, with and accompanying power supply, has been developed as an integrated device at the Zhejiang University [27, 28]. This cold plasma jet has so far been used for treatment of various biosamples at different conditions. It operates with a microsecond voltage pulse characterized with a relatively fast rise time ( $< 500$  ns). In this work, the primary aim is the spectroscopic investigation of this plasma source to the purpose of studying the streamer space–time development, morphology, and plasma parameters near the target. Optical emission spectroscopy was accompanied by electrical measurement.

## 2 Experimental setup

The cold plasma jet source, which is the subject of investigation, is devised as a complete device, consisting of a pulsed power supply and a dielectric barrier discharge (DBD) jet reactor—see the details in [28]. The electrode configuration along with image of the formed plasma plume is given in Fig. 1. The grounded electrode is a metal nozzle with its inner surface covered by a quartz tube, 6 mm in diameter. Inside the nozzle, at its center axis, a smaller quartz tube is placed, 4 mm in diameter. The high-voltage wire electrode is inserted in the smaller quartz tube. In this way, a barrier discharge is formed between the two quartz tubes having 0.5 mm thickness. The low-temperature plasma jet then protrudes from the nozzle with the diameter of  $\sim 4$  mm and length of 1–7 cm depending on the voltage. In this experiment, it was necessary to obtain a spatially stable plasma for spectroscopic measurements; therefore, a copper plate was used as a grounded target to increase the jet stability. The target was placed at a distance of 13.5 mm from the jet nozzle, though test measurements were also made with 19 mm distance.

The applied voltage on the electrode was supplied by a pulsed power source with a pulse width of  $\approx 0.8$   $\mu$ s, amplitude voltage of 2.6 kV and a repetition rate of  $f = 21$  kHz. Helium flow of 99.996% purity was controlled by means of a mass flow controller at a rate of 3 l/min. The voltage was measured using the Tektronix P6015A high-voltage probe, and current is determined from the voltage drop over 200  $\Omega$  non-inductive resistor, connected in series with the discharge.

A quartz lens was used to project the jet image onto the entrance slit of the spectrometer. The overall time-integrated emission spectra in a wide range of 200–900 nm were recorded using a low-resolution spectrometer Ocean Optics USB4000. The spatiotemporally resolved measurements were done using the Solar MSDD 1000 spectrometer with the focal length of 1 m and the grating of 1200 grooves/mm. At the exit of the monochromator, the light was detected using

the ICCD camera (PI-MAX2, Princeton Instruments) with  $1024 \times 1024$  pixels. The camera was triggered using a time-delayed pulse signal, initially generated by the rising slope of the discharge voltage pulse. The delay camera triggering system enabled precise setting of the gate width and the delay time for the recording. The used spectrometer system has an instrumental halfwidth FWHM = 0.04 nm, with pixel to pixel-to-pixel wavelength difference 0.0108 nm/pixel.

This detection system (spectrometer with ICCD camera in the gate mode) was used for the measurement of streamer development. Gate exposure time was 20 ns, with 250,000 exposures divided into 5 on-chip accumulations. Electric field strength near the target was estimated from Stark polarized spectroscopy of He I 492.2 nm using a plastic polarizer mounted at the entrance slit of the spectrometer. The latter measurement required much longer time of exposure of 200 ns.

## 3 Results and discussion

Several spectroscopic methods, typical for examining atmospheric pressure discharges, were employed in this experiment. Namely, axial distributions of various species emissions were used to examine the jet spatial structure. Helium and oxygen atomic line emission were used to examine the discharge axial development in time and measure the streamer velocity. By measuring the transverse light intensity distribution and applying the Abel transform, the radial distribution of light intensity was obtained. The  $N_2^+$  first negative system emission band was used to measure the molecule rotational temperature. Stark polarization spectroscopy of He I 492.2 nm line was used to estimate the electric field above the target.

### 3.1 Electric measurements

Voltage and current waveforms for a typical applied voltage pulse are given in Fig. 2a. The maximum voltage of 2.6 kV is reached after a relatively fast rise time of 390 ns. It can be seen that the current increase starts at the time of voltage maximum. It will be shown in the next subsection that this moment corresponds to the time when the guided streamer is initiated near the nozzle (here marked as  $t = 0$  ns). The maximum current of 36.5 mA is reached after 330 ns from its onset. The displacement current was measured by measuring the current passing through the reactor without the helium gas flow, i.e., without plasma. It was found that the displacement current is lower than 1 mA and therefore has negligible contribution to the measured current. The impedance at current maximum is estimated as voltage to current ratio at 60 k $\Omega$ —a value corresponding to the DBD reactor inside the nozzle. Figure 2b shows the change in instantaneous power obtained as voltage–current product, while its integral gives the energy of  $\varepsilon = 34$   $\mu$ J per pulse. Such low energy should provide safe treatment of biosamples. The average power can be

**Fig. 1** Experimental setup for spectroscopical observation, image of the jet and diagram of reactor configuration (*OF* optical fiber, *L* lens)

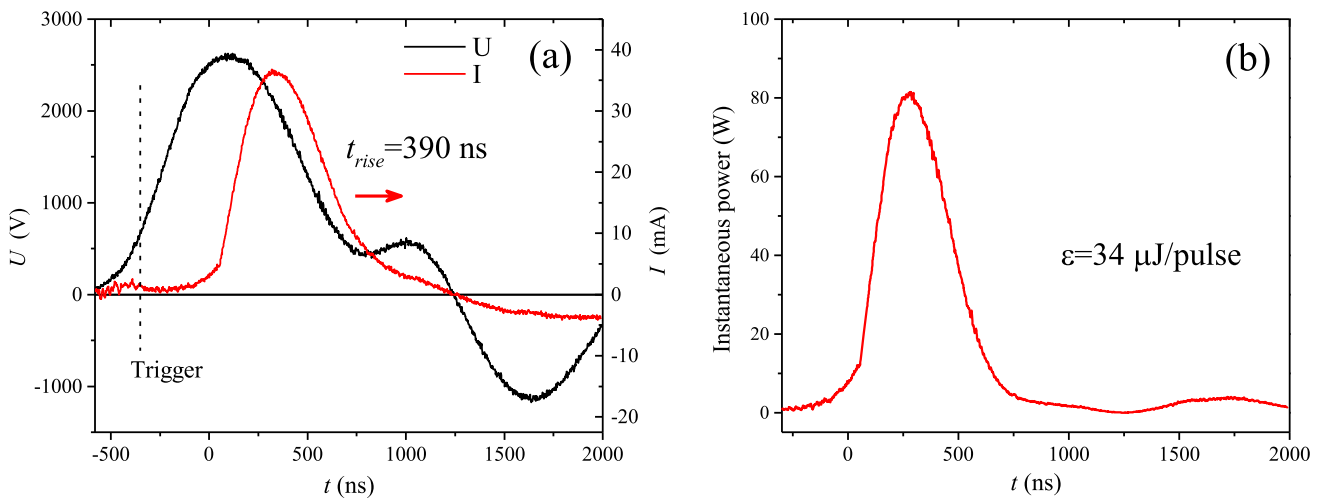
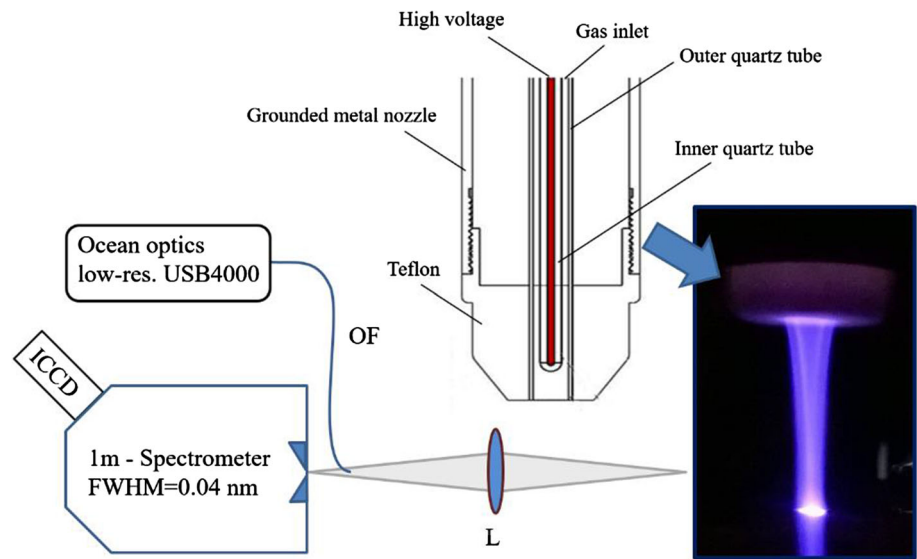


**Fig. 2** **a** Measured voltage and current waveform, **b** dissipated power in time

obtained as by multiplying energy per pulse with the repetition rate  $P = f\varepsilon = 0.71 \text{ W}$ .

### 3.2 Streamer development

To examine the streamer formation and dynamics, emission space–time intensity from atomic helium and oxygen was recorded. Figure 3a shows the space–time development of He I 706.5 nm ( $3^3\text{S}-2^3\text{P}$ ) line intensity. Since this line is excited via direct electron impact, this contour graph can be taken as representation of dynamics of the jet streamer. As can be seen, the graph shows typical features of the positive guided streamer [16, 29]. Specifically, the streamer is initially formed near the nozzle, about the time of voltage maximum, and then propagates in a “bullet-like” manner toward the cathode during the current rise. The grounded target is reached at the moment of current maximum—160 ns. After reaching the target, a weak counter-propagating

plasma ionization front is formed toward the jet nozzle [30, 31]. In continuation, during the high current value, a long-lived atmospheric pressure glow discharge above the target is formed, lasting  $\approx 600 \text{ ns}$ . This period, after the 180 ns time instance, is characterized by almost stable, but weak, light intensity in the region above the target.

On the other hand, the oxygen O I 777.4 nm ( $3^5\text{P}-3^5\text{S}$ ) development given in Fig. 3b, shows a different picture. This can be expected at high pressure, since oxygen atomic lines must be excited in a two-step process, which firstly requires dissociation of  $\text{O}_2$  molecule and subsequent electron excitation. Additionally, unlike He I 706.5 nm, its intensity is not determined only by electron density and electric field but by the presence of oxygen from the surrounding air. These effects explain the delay of the O I excitation and the time spread of its emission compared to He I line. Nevertheless, both lines show a similar time of streamer propagation. Therefore,

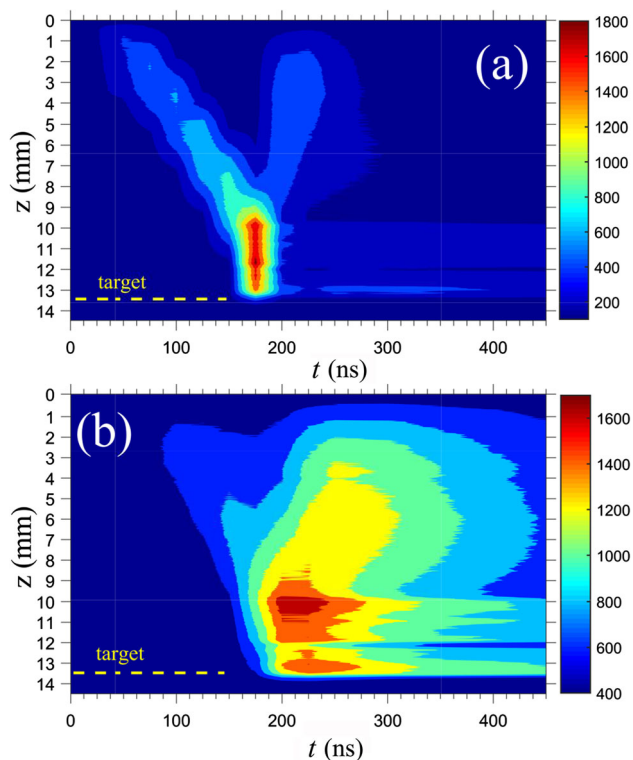


**Fig. 3** Spatiotemporal contour plot of streamer dynamics from atomic line emissions: **a** Helium He I 706.5 nm and **b** Oxygen triplet O I 777.4 nm. Gate time width = 25 ns

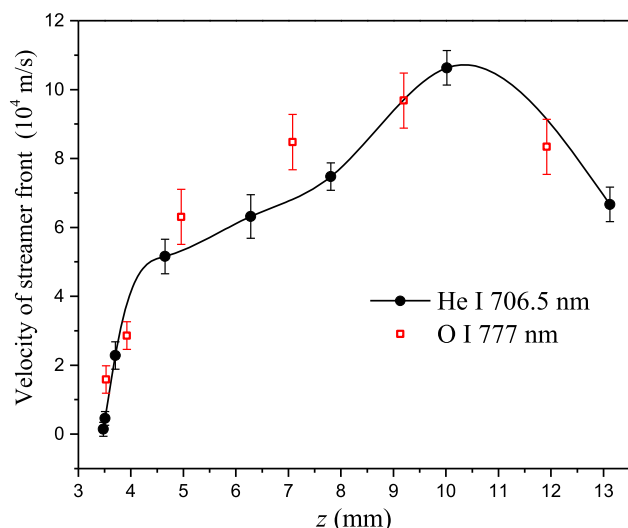


**Fig. 4** Velocity of streamer front obtained from emission of two atomic lines in Fig. 3

we have used both lines to obtain the guided streamer velocity. The obtained velocity along the axial coordinate is given in Fig. 4 from both atomic lines.

It can be seen from the graph that velocity varies from  $2 \cdot 10^4$  to  $11 \cdot 10^4$  m/s. The velocity increases with distance from the nozzle up to 11 mm and then reduces near the target. This behavior was also reported for

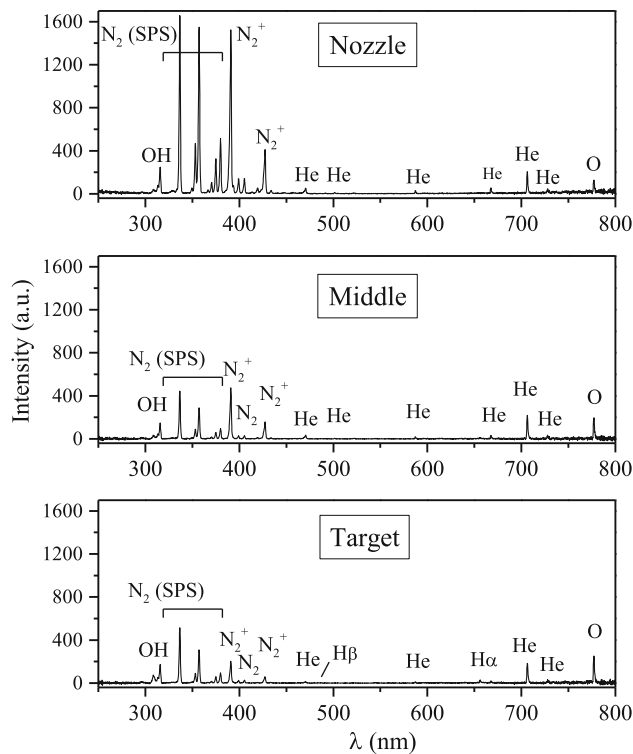


**Fig. 5** Overall emission spectrum at three axial positions

other jets, see for instance [22]. It is interesting to note that the velocity reached in this experiment is higher by a factor of 3 compared to the typical sinusoidal jet streamer velocity, see for instance [16, 29]. This effect is caused by the short rise time of the voltage in our case. Namely, it was shown in [22, 32] that the short voltage rise time crucially increases the streamer velocity. The velocity obtained here agrees with the trends given in the mentioned papers.

### 3.3 Overall spectra survey

To identify the atomic and molecular species, the overall emission spectrum was recorded at different axial positions. The low-resolution time-integrated spectrum is given in Fig. 5. Three characteristic positions are chosen. It can be seen that near the nozzle the helium atomic emissions are present across the spectrum. The  $N_2^+$  first negative system (FNS) and  $N_2$  second positive system (SPS) are the strongest emissions. At the middle of the jet plume and near the target, there is a reduction of concentration of reactive OH molecule and nitrogen molecular emission. Near the target, the presence of OH is clearly seen. The presence of reactive species (RONS) is important for treatment of biosamples. The persistent atomic oxygen line is strong in the entire jet while hydrogen Balmer series emerges from the noise only near the target. It should be noted that we did not observe NO molecular bands in the spectrum at present conditions. Similar result was obtained by Wu et al. [32] also with fast voltage rise.

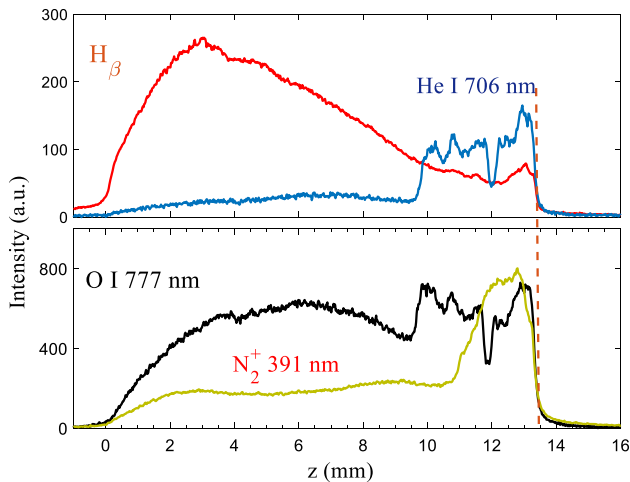


**Fig. 6** Axial distribution of emission from different species after  $t = 200$  ns. The gate time was 100 ns for all emissions except for  $N_2^+$  at 200 ns

### 3.4 Emissions axial distributions

As shown in Sect. 3.2, the very fast jet propagation requires a very short gate time of exposition for the camera, specifically at least 25 ns. For this reason, the weaker lines and bands of the spectrum could not be analyzed in the sense of development, since they require a much longer gate time to be recorded. Therefore, comparison of axial distributions of different emissions was only possible in the late stage of streamer development, when a stable emission pattern is formed above the target, see Fig. 3. Figure 6 shows the spatial distribution of different species emission, in the time when streamer has reached the target and a stable atmospheric pressure discharge is formed, lasting for several hundreds of ns. The light emissions of different species show similar patterns. Especially interesting is the formation of light and dark zones, typical for glow discharge in the vicinity of the target, see He I and O I distributions. In upper region, near the nozzle, all emissions show the trail of low intensity from the back streamer, formed in the late stage, see Fig. 3. The distributions resemble those reported in [33] for sinusoidal voltage jet.

The exception to the shape of the distribution is hydrogen  $H_\beta$  line. It is well known that at atmospheric pressure, the hydrogen Balmer lines have a delayed excitation due to the necessity of molecule dissociation and additional excitation from helium metastables [34]. This behavior was also observed in our experiment, since  $H_\beta$  did not show any intensity in the early stage of the streamer development. The shape of O I 777 also shows comparably stronger intensity in the upper part due to the delayed excitation, caused by preceding dissociation of  $O_2$  molecule, as shown in Sect. 3.2. While the time-integrated spectra in Fig. 5 show appearance of hydrogen Balmer lines only near the target, Fig. 6 shows relatively stronger intensity of  $H_\beta$  in the middle of the jet plume. This apparent discrepancy is caused by

the prolonged excitation of  $H_\beta$  in the zone of glow discharge above the target, which is accumulated in time-integrated spectrum, while the short-lived intensity in the middle does not contribute significantly to the time-integrated spectrum. It is well documented in barrier discharges at atmospheric pressure that  $H_\beta$  is weakly excited at the time of current maximum, and that it has a delayed and prolonged excitation by helium metastables [34, 35]. It should be noted that  $H_\beta$  was chosen to represent the hydrogen Balmer series emission because it could be recorded in the same wavelength window with the He lines used for Stark spectroscopy, see 3.7.

### 3.5 Gas temperature near the target

Rotational temperatures of nitrogen  $N_2$  molecule and  $N_2^+$  molecular ion are commonly taken as a measure of translational gas temperature, presuming equilibrium between the two degrees of freedom. Specifically, the rotational temperature obtained from the SPS transition  $N_2$  ( $C^3\Pi_u-B^3\Pi_g$ ) (0-0) in most cases yields the gas temperature, and it is the most used band for gas temperature determination [36]. The drawback of its use may occur in the case of a thin plasma channel, where intensive excitation in the cold region, that surrounds the active plasma, could interfere with the result [36]. On the other hand, the ion's FNS  $N_2^+$  ( $B^2\Sigma_u-X^2\Sigma_g$ ) (0-0), is emitted within the plasma channel but can suffer from non-equilibrium distribution. If the  $N_2^+$ (B) level is populated purely via electron excitation, the FNS rotational distribution yields gas temperature [36]. In the case of excitation via Penning ionization with He metastables, the rotational temperature is typically higher 30–50 K than gas temperature [36, 37]. The FNS was successfully used for gas temperature determination in DBDs [38–40] including jet [33].

Due to the sensitivity curve of our spectrometer dropping rapidly at short wavelengths, we were not able to measure the  $N_2$  SPS at 337 nm with sufficient signal-to-noise ratio. Consequently, we chose the  $N_2^+$  FNS at 391 nm which could be detected with higher intensity. Additionally, lower spectral resolution is sufficient for line separation of FNS. Due to the high velocity of the streamer, valuable measurements were only possible in the region up to 3 mm above the target, in the period after the streamer reached the target ( $t > 200$  ns). We have applied the massiveOES software [41, 42] for fitting with simulated spectrum and for forming a Boltzmann plot.

In Fig. 7, the measured FNS band 1 mm above target is shown together with the best-fit simulation. The discrepancy of the fit at shorter wavelengths comes from the low intensities of these lines but also from partially established equilibrium. By fitting the stronger lines (lower rotational levels), a Boltzmann plot was



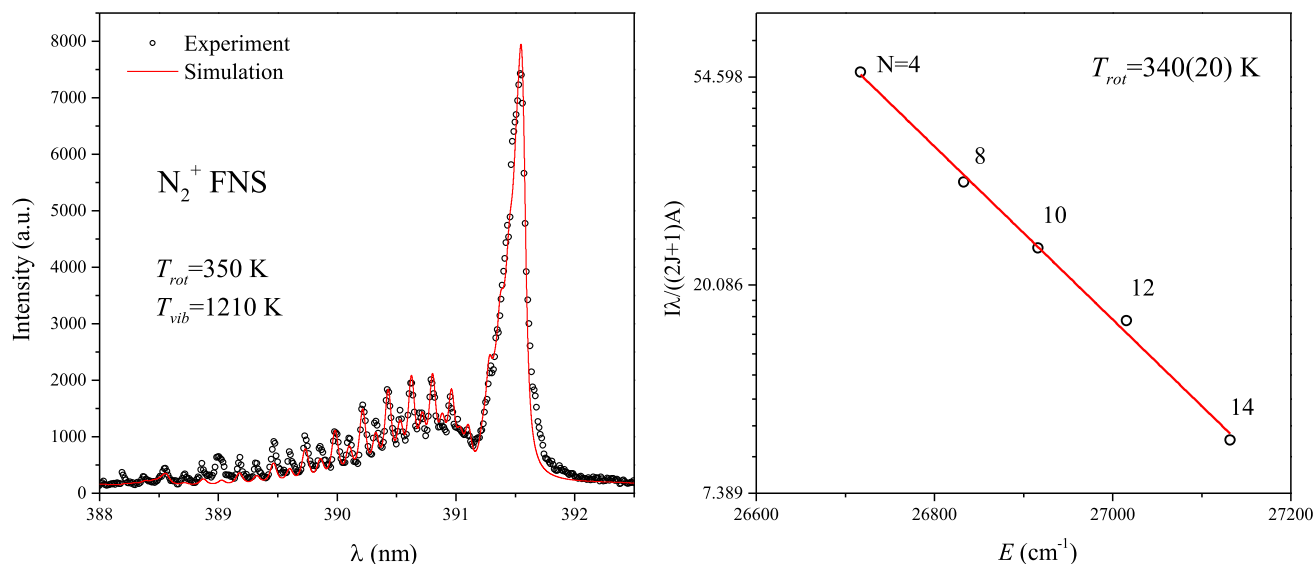


**Fig. 7** Left: measured  $N_2^+$  FNS fitted with simulated spectrum 1 mm above the target. Right: Boltzmann plot from the measured band. “massiveOES” was used

created, using the option in the massiveOES. The simulated curve shows  $T_{rot} = 350$  K, while the Boltzmann plot gives the  $T_{rot} = (340 \pm 20)$  K. These temperatures are significantly higher than room temperature, which is not expected for our low-temperature plasma source. This exceed may be explained by the use of a highly conductive target, see [43], but also by the above-mentioned excitation of  $N_2^+(B)$  in the Penning processes. To additionally estimate the gas temperature, we have measured the widths of atomic lines He I 667 nm and 728 nm. Recently, a method was suggested for precise measurement of gas temperature via Van der Waals and resonant broadening of these lines in Ref. [44]. From the Lorentz widths of the spectral profiles, we estimate the gas temperature near the target in the interval 320–330 K. This estimation agrees with the presumption of Penning excitation of  $N_2^+$  near the target. Accurate determination of  $T_{gas}$  from He lines broadening requires more careful experimental examination and is planned for future studies.

### 3.6 Radial structure of the streamer

By rotating the reactor by a right angle in front of the high-resolution spectrometer, the transverse intensity was measured at two positions and two time instances: at an early stage of streamer development (50 ns), and when it has reached the target (200 ns). Again, the line He I 706.5 nm was chosen due to electronic impact excitation of this transition.

The Abel transform was applied in order to obtain the radial intensity distribution from the line of sight transverse recording. We have used a Fourier-based Abel inversion procedure provided by Carsten Killer [45], utilizing the method given in Ref. [46]. The obtained light intensity distributions are shown in Fig. 8 for two above-mentioned times at positions  $z = 1$  mm

and  $z = 12$  mm. It can be seen that in the early stage of development, the streamer has a homogeneous density near the nozzle ( $z = 1$  mm). At a later time, the tail of the streamer at the nozzle becomes slightly more structured, see Fig. 3 for reference. On the other hand, near the target ( $z = 12$  mm) the development of streamer structure is clearly seen. Namely, as the streamer reaches the grounded target, a ring-shaped distribution is formed at 200 ns. In other words, a distinct maximum is formed at the plume periphery. The streamer diameter is also reduced toward the target. Similar conclusions can be drawn from the jet appearance in time-integrated photography (Fig. 1), i.e., a seemingly radial structure, narrowing toward the target. Since the intensity of He I line depends on local electron density and electric field strength, it may be concluded that these quantities are higher at the periphery obeying a ring-shape. Our results agree well with the results of radial investigation of a sinusoidal voltage jet in Ref [33].

### 3.7 Electric field above the target

The macroscopic electric field of the streamer was investigated using Stark polarization spectroscopy. The method is based on the Stark shifts of two helium lines in the presence of strong electric field: the allowed He I ( $4^1D-2^1P$ ) at 492.2 nm, and the forbidden He I ( $4^1F-2^1P$ ) at 492.06 nm, see Refs. [47, 48]. The method used here is already well established and applied in various discharges both at low and atmospheric pressure [48–50], including plasma jets [16, 19, 51, 52]. Namely, the jet radiation polarized in the field direction ( $\pi$ -polarization) is recorded and then the measured spectrum is fitted in the vicinity of 492 nm. The fitting function includes the forbidden and allowed line with their shifts correlated to the field using tables in

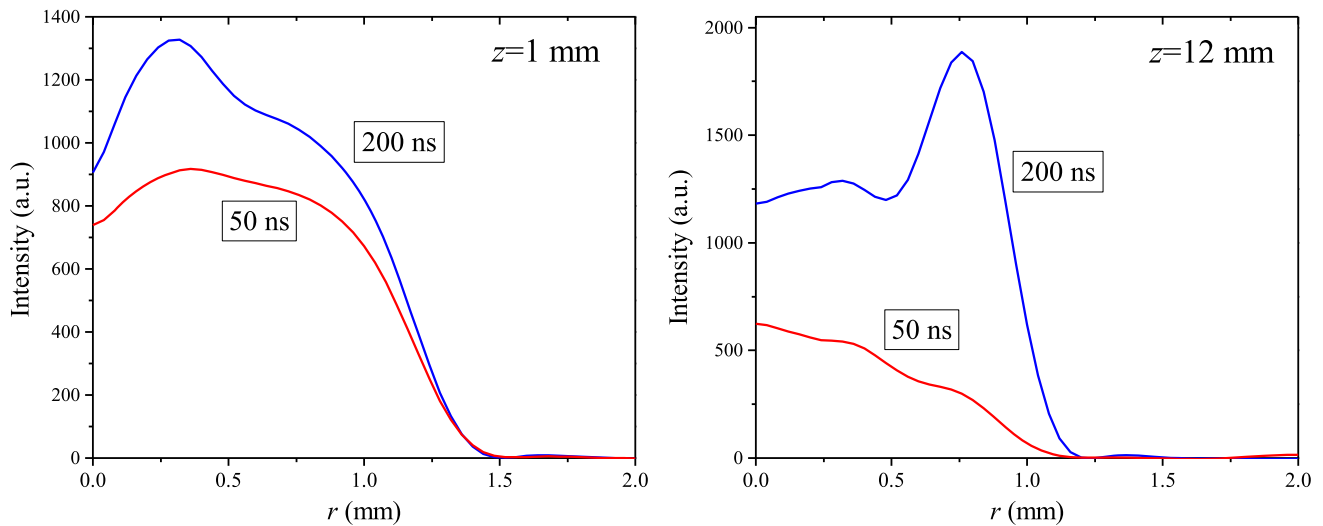


**Fig. 8** Radial distributions of He I 706.5 nm intensity at two positions and two time instances: left near the nozzle ( $z = 1$  mm), and near the target ( $z = 12$  mm)

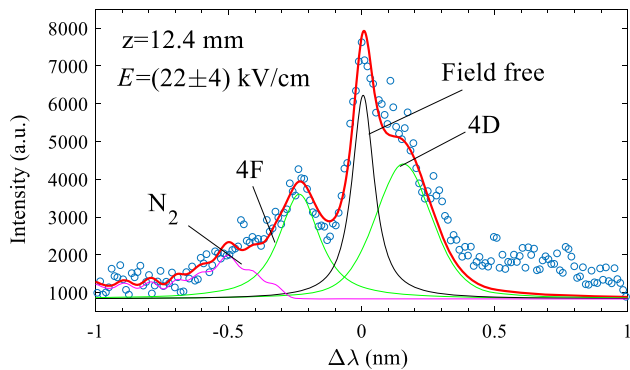


**Fig. 9** Example of the fitted  $\pi$ -polarized spectrum in the vicinity of He I 492.2 nm. Dots experimental points; full lines fit

[48]. Additionally, the fitting function in some cases must include a field-free component emitted by excited atoms out of the strong-field region, see the details [50]. In our case, the fitting function included all of the three above-mentioned He line components as pseudo-Voigt profile functions. In addition, the  $N_2$  molecular band (SPS) at 491.68 nm was included, with position and shape taken from massiveOES [41] and tables [53]. An example of measured  $\pi$ -polarized profile with accompanying fit is given in Fig. 9. The profile clearly shows that the allowed line is much broader than the expected value: allowed is FWHM = 0.25 nm, compared 0.1 nm for field-free. Furthermore, the allowed line shows an asymmetric shape with a strong red tail, which could not be fitted with the utilized function. All this clearly indicates the presence of a strong electric field, with inhomogeneity along the line of sight. Consequently, the electric field calculated from the fit carries high uncertainty. More precise field value, and a clearer picture, could be obtained using Abel inversion and/or detailed

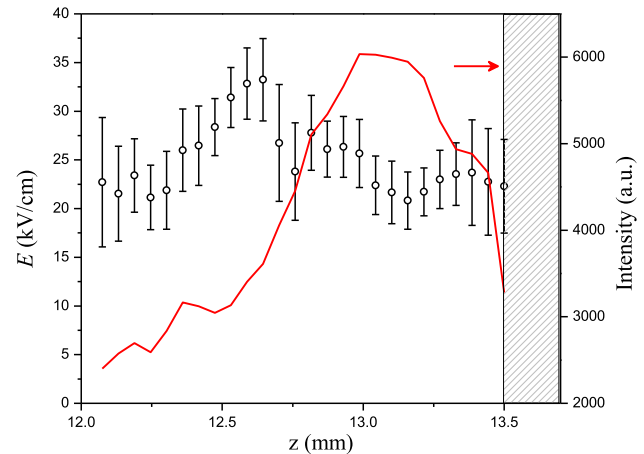


**Fig. 10** The obtained electric field distribution above the target with intensity of forbidden and allowed He I line. Shaded rectangle is the target surface

analysis of the spectrum, similar to the ones in Refs. [54, 55]. However, this was not possible due to the very low intensity of He I 492.2 nm and its forbidden counterpart.

The estimated electric field distribution above the target is given in Fig. 10. It should be noted that it was not possible to measure the required He lines with short gate width; therefore, we were not able to measure the field during the rapid propagation of the streamer, but only in the vicinity of the target, when a quasi-stable glow discharge is formed. The centered field strength, within the uncertainty interval, varies from 23 to 33 kV/cm. The field reaches significantly higher values than those obtained in sinusoidal voltage jet [16, 19], while it is close to the value reached in nanosecond pulse jet with grounded glass target [52]. The shape of the distribution is not clear due to high uncertainty,

but corresponds well to the distributions near the target given in [16, 52]. Furthermore, our results of electric field strength agree well with the modeling and experimental study of a microsecond pulse helium jet by Bourdon et al. [56]. Specifically, the authors have obtained a peak field of 45 kV/cm compared with 33 kV/cm in Fig. 10, but using a much higher voltage amplitude than the present.

## 4 Conclusion

A cold helium plasma jet reactor, devised as a device for treatment of biosamples, is studied experimentally to obtain the knowledge of its streamer parameters and structure. The key feature of this setup is a microsecond pulse voltage supply with a rise time  $\approx 400$  ns. The experimental study was based on several methods of optical emission spectroscopy accompanied with electrical measurement. The spatiotemporally resolved spectroscopy showed a fast propagating guided streamer with velocity reaching  $10^5$  m/s near the target. The axial intensity of different spectral transitions, after the current maximum is reached, revealed a quasi-stable glow-like discharge formed above the target with a reconnection channel. Gas temperature, obtained from rotational spectra, was higher than expected probably due to the use of conductive target. Radial radiation distributions, obtained by Abel inversion, displayed a ring-shaped streamer structure, in accordance with previous experiments. Electric field distribution could only be measured above the target and showed an expected shape, reaching 33 kV/cm. Compared to the sinusoidal jet, this experiment showed a much higher streamer velocity and significantly higher electric field strength. These effects can be attributed to a fast rise time of the applied voltage pulse. It can be concluded that variation of pulse voltage rise time of the order of hundreds of ns could be used to control the streamer plasma parameters.

**Acknowledgements** Preliminary results of this study were partially presented at the conference SPIG 2020 as a poster presentation, and published in the conference proceedings. This work was supported by the Ministry of Education and Science of the Republic of Serbia within the projects 451-03-47/2023-01/ 200162 and /200128.

## Author contribution

All authors contributed equally to this work.

**Data Availability Statement** This manuscript has associated data in a data repository. [Authors' comment: The datasets generated during and/or analyzed during the current study are available from the corresponding author on reasonable request.]

## References

1. G. Fridman, G. Friedman, A. Gutsol, A.B. Shekhter, V.N. Vasilets, A. Fridman, Applied plasma medicine. *Plasma Process. Polym.* **5**, 503–533 (2008)
2. R. Brandenburg, A. Bogaerts, W. Bongers, A. Fridman, G. Fridman, B.R. Locke, V. Miller, S. Reuter, M. Schiorlin, T. Verreycken, K. Ostrikov, White paper on the future of plasma science in environment, for gas conversion and agriculture. *Plasma Process Polym.* **16**, 1–18 (2019)
3. J. Winter, R. Brandenburg, K.D. Weltmann, Atmospheric pressure plasma jets: an overview of devices and new directions. *Plasma Sources Sci, Technol.* **24**, 64001 (2015)
4. K.D. Weltmann, T. Von Woedtke, Plasma medicine—current state of research and medical application. *Plasma Phys. Control. Fusion* **59**, 014031 (2017)
5. S. Reuter, T. Von Woedtke, K.D. Weltmann, The kIN-Pen—a review on physics and chemistry of the atmospheric pressure plasma jet and its applications. *J. Phys. D Appl. Phys.* **51**, 233001 (2018)
6. Y. Lu, S. Wu, W. Cheng, X. Lu, Electric field measurements in an atmospheric-pressure microplasma jet using Stark polarization emission spectroscopy of helium atom. *Eur. Phys. J. Spec. Top.* **226**, 2979–2989 (2017)
7. A.V. Nastuta, I. Topala, C. Grigoras, V. Pohoata, G. Popa, Stimulation of wound healing by helium atmospheric pressure plasma treatment. *J. Phys. D. Appl. Phys.* **44**, 105204 (2011)
8. M. Laroussi, X. Lu, M. Keidar, Perspective: the physics, diagnostics, and applications of atmospheric pressure low temperature plasma sources used in plasma medicine. *J. Appl. Phys.* **122**, 020901 (2017)
9. T. Von Woedtke, S. Emmert, H.R. Metelmann, S. Rupf, K.D. Weltmann, Perspectives on cold atmospheric plasma (CAP) applications in medicine. *Phys. Plasmas* **27**, 070601 (2020)
10. A. Khlyustova, C. Labay, Z. Machala, M.P. Ginebra, C. Canal, Important parameters in plasma jets for the production of RONS in liquids for plasma medicine: a brief review. *Front.Chem. Sci. Eng.* **13**, 238–252 (2019)
11. V. Vijayarangan, A. Delalande, S. Dozias, J.M. Povesle, C. Pichon, E. Robert, Cold atmospheric plasma parameters investigation for efficient drug delivery in HeLa cells. *IEEE Trans. Radiat. Plasma Med. Sci.* **2**, 109–115 (2018)
12. V. Vijayarangan, A. Delalande, S. Dozias, J.-M. Povesle, E. Robert, C. Pichon, New insights on molecular internalization and drug delivery following plasma jet exposures. *Int. J. Pharm.* **589**, 119874 (2020)
13. T. Chung, A. Stancampiano, K. Sklias, K. Gazeli, F. André, S. Dozias, C. Douat, J. Povesle, J. Santos Sousa, É. Robert, L. Mir, Cell Electroporation enhancement by Non-Thermal-Plasma-Treated PBS. *Cancers (Basel)* **12**, 219 (2020)
14. Q. Zhang, J. Zhuang, T. Von Woedtke, J.F. Kolb, J. Zhang, J. Fang, K.D. Weltmann, Synergistic antibacterial effects of treatments with low temperature plasma jet and pulsed electric fields. *Appl. Phys. Lett.* **105**, 104103 (2014)



15. J.P. Boeuf, L.L. Yang, L.C. Pitchford, Dynamics of a guided streamer ('plasma bullet') in a helium jet in air at atmospheric pressure. *J. Phys. D. Appl. Phys.* **46**, 15201 (2013)
16. G.B. Sretenović, I.B. Krstić, V.V. Kovačević, B.M. Obradović, M.M. Kuraica, Spatio-temporally resolved electric field measurements in helium plasma jet. *J. Phys. D Appl. Phys.* **47**, 102001 (2014)
17. G.B. Sretenović, I.B. Krstić, V.V. Kovačević, B.M. Obradović, M.M. Kuraica, The isolated head model of the plasma bullet/streamer propagation: Electric field-velocity relation. *J. Phys. D. Appl. Phys.* **47**, 355201 (2014)
18. A. Sobota, O. Guaitella, G.B. Sretenović, I.B. Krstić, V.V. Kovačević, A. Obrusník, Y.N. Nguyen, L. Zajíčková, B.M. Obradović, M.M. Kuraica, Electric field measurements in a kHz-driven He jet—the influence of the gas flow speed. *Plasma Sources Sci. Technol.* **25**, 065026 (2016)
19. A. Sobota, O. Guaitella, G.B. Sretenović, V.V. Kovačević, E. Slikboer, I.B. Krstić, B.M. Obradović, M.M. Kuraica, Plasma-surface interaction: Dielectric and metallic targets and their influence on the electric field profile in a kHz AC-driven He plasma jet. *Plasma Sources Sci. Technol.* **28**, 045003 (2019)
20. G.B. Sretenović, P.S. Iskrenović, I.B. Krstić, V.V. Kovačević, B.M. Obradović, M.M. Kuraica, Quantitative analysis of plasma action on gas flow in a He plasma jet. *Plasma Sources Sci. Technol.* **27**, 07LT01 (2018)
21. P. Viegas, E. Slikboer, Z. Bonaventura, O. Guaitella, A. Sobota, A. Bourdon, Physics of plasma jets and interaction with surfaces: review on modelling and experiments. *Plasma Sources Sci. Technol.* **31**, 053001 (2022)
22. X. Lu, G.V. Naidis, M. Laroussi, K. Ostrikov, Guided ionization waves: theory and experiments. *Phys. Rep.* **540**, 123–166 (2014)
23. Z. Xiong, M.J. Kushner, Atmospheric pressure ionization waves propagating through a flexible high aspect ratio capillary channel and impinging upon a target. *Plasma Sources Sci. Technol.* **21**, 034001 (2012)
24. M. Gherardi, N. Puač, D. Marić, A. Stancampiano, G. Malović, V. Colombo, Z.L. Petrović, Practical and theoretical considerations on the use of ICCD imaging for the characterization of non-equilibrium plasmas. *Plasma Sources Sci. Technol.* **24**, 064004 (2015)
25. E. Robert, V. Sarron, D. Riès, S. Dozias, M. Vandamme, J.-M. Pouvesle, Characterization of pulsed atmospheric-pressure plasma streams (PAPS) generated by a plasma gun. *Plasma Sources Sci. Technol.* **21**, 034017 (2012)
26. Y. Morabit, R.D. Whalley, E. Robert, M.I. Hasan, J.L. Walsh, Turbulence and entrainment in an atmospheric pressure dielectric barrier plasma jet. *Plasma Process Polym.* **17**, 1900217 (2020)
27. C. Zheng, Y. Kou, Z. Liu, A. Zhu, H. Jiang, Y. Huang, K. Yan, A microsecond-pulsed cold plasma jet for medical application. *Plasma Med.* **6**, 179–191 (2016)
28. G. Deng, Q. Jin, S. Yin, C. Zheng, Z. Liu, K. Yan, Experimental study on bacteria disinfection using a pulsed cold plasma jet with helium/oxygen mixed gas. *Plasma Sci. Technol.* **20**, 115503 (2018)
29. T. Gerling, A.V. Nastuta, R. Bussiahn, E. Kindel, K.-D. Weltmann, Back and forth directed plasma bullets in a helium atmospheric pressure needle-to-plane discharge with oxygen admixtures. *Plasma Sources Sci. Technol.* **21**, 034012 (2012)
30. T. Darny, J.-M. Pouvesle, V. Puech, C. Douat, S. Dozias, E. Robert, Analysis of conductive target influence in plasma jet experiments through helium metastable and electric field measurements. *Plasma Sources Sci. Technol.* **26**, 045008 (2017)
31. R.S. Sigmond, The residual streamer channel: Return strokes and secondary streamers. *J. Appl. Phys.* **56**, 1355–1370 (1984)
32. S. Wu, H. Xu, X. Lu, Y. Pan, Effect of pulse rising time of pulse dc voltage on atmospheric pressure non-equilibrium plasma. *Plasma Process Polym.* **10**, 136–140 (2013)
33. G.B. Sretenović, I.B. Krstić, V.V. Kovačević, B.M. Obradović, M.M. Kuraica, Spectroscopic study of low-frequency helium DBD plasma jet. *IEEE Trans Plasma Sci.* **40**, 2870–2878 (2012)
34. Z. Navrátil, R. Brandenburg, D. Trunec, Brablec a, St'ahel P, Wagner H-E and Kopecký Z, Comparative study of diffuse barrier discharges in neon and helium. *Plasma Sources Sci. Technol.* **15**:, 8–17 (2005)
35. S.S. Ivković, N. Cvetanović, B.M. Obradović, Experimental study of gas flow rate influence on a dielectric barrier discharge in helium. *Plasma Sources Sci. Technol.* **31**, 095017 (2022)
36. P.J. Bruggeman, N. Sadeghi, D.C. Schram, V. Linss, Gas temperature determination from rotational lines in non-equilibrium plasmas: a review. *Plasma Sources Sci. Technol.* **23**, 023001 (2014)
37. W.C. Richardson, D.W. Setser, Penning ionization optical spectroscopy: Metastable helium (He 2<sup>3</sup>S) atoms with nitrogen, carbon monoxide, oxygen, hydrogen chloride, hydrogen bromide, and chlorine. *J. Chem. Phys.* **58**, 1809–1825 (1973)
38. N.K. Bibinov, A.A. Fateev, K. Wiesemann, Variations of the gas temperature in He/N<sub>2</sub> barrier discharges. *Plasma Sources Sci. Technol.* **10**, 579–588 (2001)
39. A.S. Chiper, V. Anița, C. Agheorghiesei, V. Pohoța, M. Anița, G. Popa, Spectroscopic diagnostics for a DBD plasma in He/Air and He/N<sub>2</sub> gas mixtures. *Plasma Process Polym.* **1**, 57–62 (2004)
40. J. Muñoz, C. Yubero, M.S. Dimitrijević, M.D. Calzada, Gas temperature determination in atmospheric pressure surface wave discharges from atomic line broadening 33, 2–5 (2009)
41. J. Voráč, P. Synek, L. Potočnáková, J. Hnilica, V. Kudrle, Batch processing of overlapping molecular spectra as a tool for spatio-temporal diagnostics of power modulated microwave plasma jet. *Plasma Source Sci. Technol.* **26**, 025010 (2017)
42. J. Voráč, L. Kusýn, P. Synek, Deducing rotational quantum-state distributions from overlapping molecular spectra. *Rev. Sci. Instrum.* **90**, 123102 (2019)
43. R. Wang, H. Xu, Y. Zhao, W. Zhu, K. Ostrikov, T. Shao, Effect of dielectric and conductive targets on plasma jet behaviour and thin film properties. *J. Phys. D Appl. Phys.* **52**, 074002 (2019)
44. M.C. García, C. Yubero, A. Rodero, Gas temperature and air fraction diagnosis of helium cold atmospheric plasmas by means of atomic emission lines. *Spectrochim Acta - Part B At. Spectrosc.* **193**, 106437 (2022)

45. C. Killer, Abel inversion algorithm. *Matlabcentral - file Exch* (2022)
46. G. Pretzier, A new method for numerical Abel-inversion. *Zeitschrift für Naturforsch. A* **46a**, 639–671 (1991)
47. M.M. Kuraica, Konjević N, Electric field measurement in the cathode fall region of a glow discharge in helium. *Appl. Phys. Lett.* **70**, 1521 (1997)
48. N. Cvetanović, M.M.M. Martinović, B.M. Obradović, M.M. Kuraica, Electric field measurement in gas discharges using stark shifts of He I lines and their forbidden counterparts. *J. Phys. D Appl. Phys.* **48**, 205201 (2015)
49. B.M. Obradović, S.S. Ivković, M.M. Kuraica, Spectroscopic measurement of electric field in dielectric barrier discharge in helium. *Appl. Phys. Lett.* **92**, 3–5 (2008)
50. B.M. Obradović, N. Cvetanović, S.S. Ivković, G.B. Sretenović, V.V. Kovačević, I.B. Krstić, M.M. Kuraica, Methods for spectroscopic measurement of electric field in atmospheric pressure helium discharges ed N Gherardi and T Hoder. *Eur. Phys. J. Appl. Phys.* **77**, 30802 (2017)
51. M. Hofmans, A. Sobota, Influence of a target on the electric field profile in a kHz atmospheric pressure plasma jet with the full calculation of the Stark shifts. *J. Appl. Phys.* **125**, 043303 (2019)
52. M. Mirzaee, M. Simeni Simeni, P.J. Bruggeman, Electric field dynamics in an atmospheric pressure helium plasma jet impinging on a substrate. *Phys. Plasmas* **27**, 123505 (2020)
53. R.W.B. Pearse, A.G. Gaydon, *The Identification of Molecular Spectra* (Springer, Dordrecht, 1976)
54. Z. Navrátil, R. Josepson, N. Cvetanović, B. Obradović, P. Dvořák, Electric field development in  $\gamma$ -mode radiofrequency atmospheric pressure glow discharge in helium. *Plasma Sources Sci. Technol.* **25**, 03 (2016)
55. L. Wang, N. Cvetanović, B. Obradović, G. Dinescu, C. Leys, A.Y. Nikiforov, Investigation of atmospheric pressure RF discharge with coexisting  $\alpha$  and  $\gamma$ -modes. *Plasma Sources Sci. Technol.* **28**, 055010 (2019)
56. A. Bourdon, T. Darny, F. Pechereau, J.-M. Povesle, P. Viegas, S. Iséni, E. Robert, Numerical and experimental study of the dynamics of a  $\mu$ s helium plasma gun discharge with various amounts of N<sub>2</sub> admixture. *Plasma Sources Sci. Technol.* **25**, 035002 (2016)

Springer Nature or its licensor (e.g. a society or other partner) holds exclusive rights to this article under a publishing agreement with the author(s) or other rightsholder(s); author self-archiving of the accepted manuscript version of this article is solely governed by the terms of such publishing agreement and applicable law.